Austenitization triggering breakaway oxidation of FeCr-base alloys at 900 °C

Corrosion Science 244 (2025) 112605

Contents lists available at ScienceDirect

Corrosion Science

journal homepage: www.elsevier.com/locate/corsci

Austenitization triggering breakaway oxidation of FeCr-base alloys at 900 °C

A. Chyrkin [a,*], J. Froitzheim [a], J. Zurek [b], D. Naumenko [b]

[a] Chalmers University of Technology, Department of Chemistry and Chemical Engineering, Kemivägen 10, Gothenburg 412 58, Sweden
[b] Forschungszentrum Jülich GmbH, Institute for Energy Materials and Devices (IMD-1), Leo-Brandt-Straße, Jülich 524 25, Germany

ARTICLE INFO

Keywords:
Ferritic stainless steel
SOFC/SOEC
Breakaway oxidation
Cr_2O_3
Alloying
Diffusion
Phase transformation

ABSTRACT

Oxidation of Fe18Cr-X (X = Mo, Si) alloys in Ar-H_2-H_2O gas mixtures has been studied at 900 °C. The α-to-γ transformation at the Cr-depleted specimen edges is demonstrated to be the primary reason of breakaway oxidation. A diffusion analysis predicted protective behavior for ferritic (BCC) Fe-18Cr at 900 °C and loss of protection once austenite (FCC) is formed. Alloying Fe-18Cr with Si or coating with Ce resulted in a significantly lower oxidation rate and thus protective oxidation behavior while alloying with a ferrite stabilizing element (Mo) completely prevented breakaway oxidation not affecting the oxidation rate.

1. Introduction

Ferritic stainless steel components are commonly used for high temperature applications such as conventional power plants, exhaust parts or more recently interconnects for Solid Oxide Fuel or Electrolysis Cells (SOFC or SOEC). Chromia-forming stainless steels used in SOFC/SOEC and heat-exchangers rely for their corrosion resistance on the formation of a protective, slow-growing, well adherent Cr_2O_3 scale. This barrier of Cr_2O_3 is efficient in dry air or pure oxygen [1–4]. However, water vapor is generally known to deteriorate performance of stainless steels in both high-pO_2 [5–8] and low-pO_2 [9–13] gases promoting breakaway oxidation, i.e., rapid outward growth of Fe-rich oxides accompanied by internal oxidation.

In humid high-pO_2 atmospheres such as humid air or combustion gases, the most explored degradation mechanism is reactive evaporation of Cr [5,14–16]. While the Cr evaporation phenomenon is well understood, quantified and successfully mitigated by application of coatings [17,18], breakaway oxidation mechanism in low-pO_2 gases such as H_2/H_2O or steam [8] is still poorly understood. The topic has recently gained renewed interest with the rapid growth of SOEC technology to produce the vast amounts of hydrogen needed the green energy transition. The cathode side atmosphere in an SOEC stack is commonly a mixture of H_2 and H_2O with the H_2/H_2O ratio increasing as the gas runs through the stack. It is thus paramount to understand the parameters affecting the breakdown of the protective Cr_2O_3 scale in H_2/H_2O environments.

In H_2/H_2O gases, ferritic stainless steels demonstrate an anomalous corrosion temperature dependence [10,11], i.e., oxidation rate passes through a peak between 550 and 650 °C abating towards 750–800 °C. A similar oxidation rate pattern is reported for dual-atmosphere corrosion, i.e., an experimental setup in which a thin (0.2 mm) steel specimen serves as a wall separating air from H_2/H_2O: the air side corrosion is most intense at 600 °C [19–21].

This anomalous temperature dependence as well as the beneficial effect of cold-work promoting Cr_2O_3-growth [11] on ferritic steels in H_2/H_2O point towards a lack of Cr diffusion in the alloy as the key factor in the mechanism of "low-temperature" breakaway oxidation. At 550–650 °C, Cr diffusion in the steel is not sufficient to balance the amount of Cr lost due to oxide scale formation. However, exact mechanistic aspects of the H_2O and/or H_2 effect on the transport phenomena in Cr_2O_3 and in the alloy are still not well understood.

Apart from "low-temperature" breakaway, some steel grades suffer from "high-temperature" breakaway oxidation in H_2/H_2O at 900 °C [10] and above. Unlike "low-temperature" breakaway, this phenomenon affects only some steel grades such as AISI 430 (1.4016) while other steels grades such as AISI 441 (1.4509) or Crofer 22 APU (1.4760) formed a protective Cr_2O_3 scale in Ar-4 %H_2-20 %H_2O at 900 °C. The main compositional differences between AISI 430 (1.4016) and AISI 441 (1.4509) are the ferrite stabilizing alloying elements, e.g., Si, Ti and Nb, hence, it is reasonable to assume that an α-to-γ phase transformation due

* Corresponding author.
E-mail address: chyrkin@chalmers.se (A. Chyrkin).

https://doi.org/10.1016/j.corsci.2024.112605
Received 4 September 2024; Received in revised form 4 November 2024; Accepted 27 November 2024
Available online 30 November 2024

Table 1
Chemical composition of the alloys used in the study in wt% obtained by ICP-OES and IR.

	Fe-18Cr	Fe-18Cr-2Mo	Fe-18Cr-0.5Si	Fe-30Cr
Fe	Bal.	Bal.	Bal.	Bal.
Cr	18,59	18,3	18,2	29,2
Si	< 0007	0,0682	0362	< 0006
Al	< 0005	0.0157	< 0004	< 0003
Mn	< 0002	< 0001	< 0002	< 0001
Ni	0.0054	0.0055	0.0051	0.001
Mo	< 0001	1.834	< 0,0008	< 0002
Nb	< 0005	< 0004	< 0004	< 0002
W	< 0006	< 0004	< 0005	< 0003
Ti	< 0001	< 0,0007	< 0,0008	< 0002
Cu	< 0005	< 0004	< 0004	< 0,0005
Co	0.0018	0.0017	0.0017	0.006
Mg	< 0002	< 0001	< 0002	< 0002
P	< 0,01	< 0007	< 0008	< 0008
C	0005	0010	0008	0006
N	0004	0004	0003	0004
O	0081	0061	0059	0029

Table 2
Calculated pO_2 values for Ar-4 %H_2-2 %H_2O and Ar-4 %H_2-7 %H_2O gas mixtures as well as for the Fe/FeO equilibrium at 800 and 900 °C. The calculations were made using the thermodynamic data from [24].

T / °C	pO_2 / atm		
	Fe/FeO	Ar−4 %H_2−2 %H_2O	Ar−4 %H_2−7 %H_2O
800	1.1 x10^{-19}	1.3 x10^{-19}	1.3 x10^{-18}
900	1.7 x10^{-17}	1.5 x10^{-17}	1.8 x10^{-16}

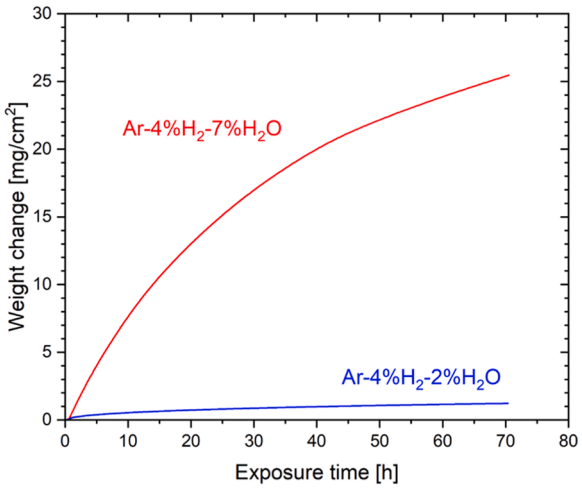

Fig. 1. In-situ weight change of Fe-18Cr exposed for 72 h to Ar-4 %H_2-2 %H_2O and Ar-4 %H_2-7 %H_2O at 900 °C in thermobalance.

to Cr-depletion may be the key phenomenon behind the "high--temperature" breakaway oxidation. The austenitization mechanism has been hypothesized in several studies [10,22] but it has never been experimentally verified.

The aim of the present work is to investigate the role of austenitization in "high-temperature" breakaway at 900°C. The austenitization effects are experimentally explored via alloying the baseline alloy Fe-18Cr (wt%), a composition close to AISI 441, with alloying additions to produce common effects in ferritic stainless steels: (i) higher Cr content (30 wt%) to stay away from the γ-loop, (ii) alloying with 2 wt% Mo to suppress austenite formation under Cr depletion at 900 °C; (iii) alloying with 0.5 wt% Si to form a subscale SiO_2 layer and thereby lower Cr-consumption/depletion, and iv) coating Fe-18Cr with Ce to reduce the oxidation rate without major alloying. The oxidation behavior of these alloys is studied in Ar-4 %H_2-2 %H_2O and Ar-4 %H_2-7 %H_2O gas mixtures at 800 and 900 °C. The difference in pH_2O in both atmospheres raises the pO_2 from 1.5 x 10^{-17} to 1.8 x 10^{-16} atm while the pO_2 of Fe/FeO equilibrium at 900 °C is 1.7 x 10^{-17} atm at 900 °C. Consequently, in the former atmosphere no Fe-oxide is stable leaving only Cr as a major scale forming element, while in the latter FeO is thermodynamically stable and will form if Cr is critically depleted at the metal-oxide interface.

2. Experimental

2.1. Materials

Model alloys for this study were supplied by HMW Hauner GmbH & Co.KG (Röttenbach, Germany). The alloys were arc-melted in vacuum from pure elements of 99,995 % purity. The ingots were hot-rolled to 2 mm thickness and further cold-rolled to 0.6 mm and 0.3 mm thick sheets. The chemical compositions of the alloys are listed in Table 1. Test coupons measuring 20 mm x 10 mm were machined from the sheets. The specimens were exposed in as-rolled state. All specimen surfaces were ground with SiC papers to 1200 grit surface finish. On several 0.3 mm thick Fe-18Cr coupons, a 10 nm Ce coating was applied using a pre-cut sheet as described in [23]. Ce was coated in a PVD process by Alleima AB (Sandviken, Sweden). The specimens were degreased with acetone and ethanol in an ultrasonic bath and dried with pressurized air prior to exposure.

2.2. Furnace exposures

The furnace exposures in Ar-4 %H_2-2 %H_2O and Ar-4 %H_2-7 %H_2O gas mixtures were carried out in an alumina tube in a horizontal furnace. The Ar-4 %H_2 gas mixture supplied by Linde Gas was bubbled through a humidifier kept at 17.5 and 39.1 °C, respectively. The pO_2 values for both gases at 800 and 900 °C are listed together with those for Fe/FeO equilibria in Table 2. The equilibrium constants as well as the pO_2 values were calculated using the thermodynamic data from [24].

The alloy specimens were introduced into a cold furnace, flushed with the dry Ar-4 %H_2 gas for 1 h and heated at 10 K min^{-1} per minute to reach the exposure temperature. The humidification was turned on once the furnace reached the target temperature. The cooling rate was 10 K min^{-1} as well. The gas flow rate was set at 200 ml min^{-1}. In every furnace exposure, four alloy coupons were exposed to determine the average mass change and the measurement error.

2.3. Thermobalance exposures

The *in-situ* oxidation kinetics measurements were isothermally performed with a SETARAM thermobalance in flowing Ar-4 %H_2-2 %H_2O and Ar-4 %H_2-7 %H_2O gas mixtures for up to 72 h at 900 °C. The heating rate was 90 K min^{-1}. The cooling rate was 10 K min^{-1}.

2.4. Microstructural analyses

The exposed specimens were sectioned, gold-sputtered, electrochemically Ni-plated and hot-mounted in a conductive Polyfast mounting resin supplied by Struers (Copenhagen, Denmark) or non-conductive epoxy resins. The mounted cross-sections were subsequently ground with SiC paper to 4000 grit and polished to 0.25 μm surface finish. The final etching step was performed using either colloidal silica or the Hitachi ArBlade 500 ion milling system. FEI Quanta 200 ESEM and Zeiss Ultra electron microscopes equipped with an energy dispersive X-ray spectrometer (EDS) were used for post-exposure analyses.

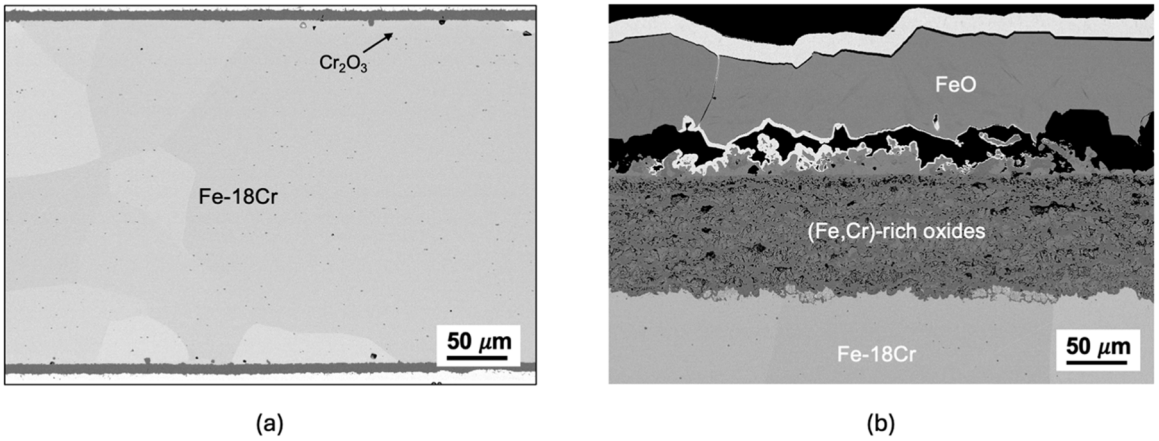

Fig. 2. BSE images of cross-sectioned Fe-18Cr alloy specimens exposed for 72 h at 900 °C in (a) Ar-4 %H_2-2 %H_2O and (b) Ar-4 %H_2-7 %H_2O.

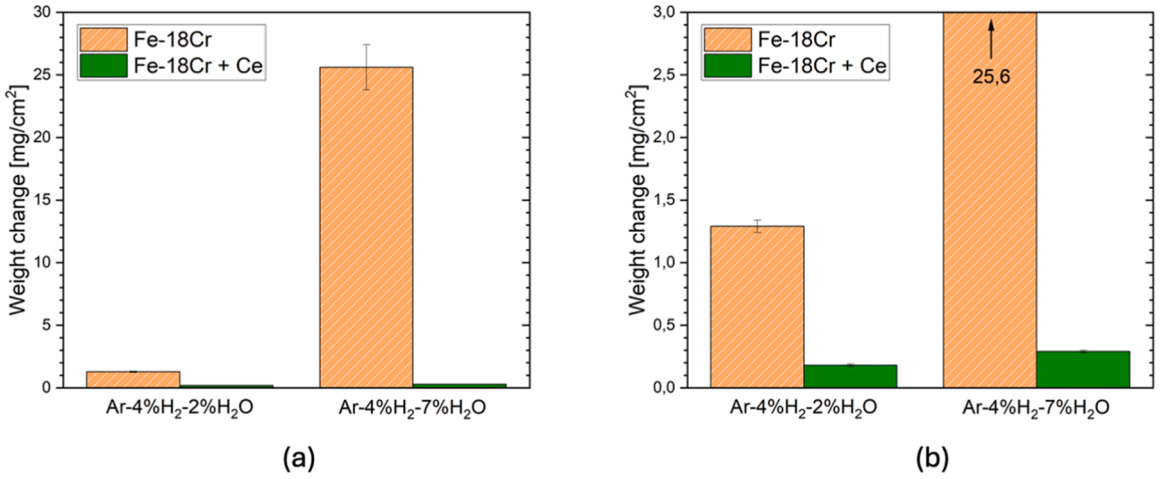

Fig. 3. Weight change of bare and Ce-coated Fe-18Cr specimens exposed for 72 h in Ar-4 %H_2-2 %H_2O and Ar-4 %H_2-7 %H_2O at 900 °C in a horizontal tube furnace.

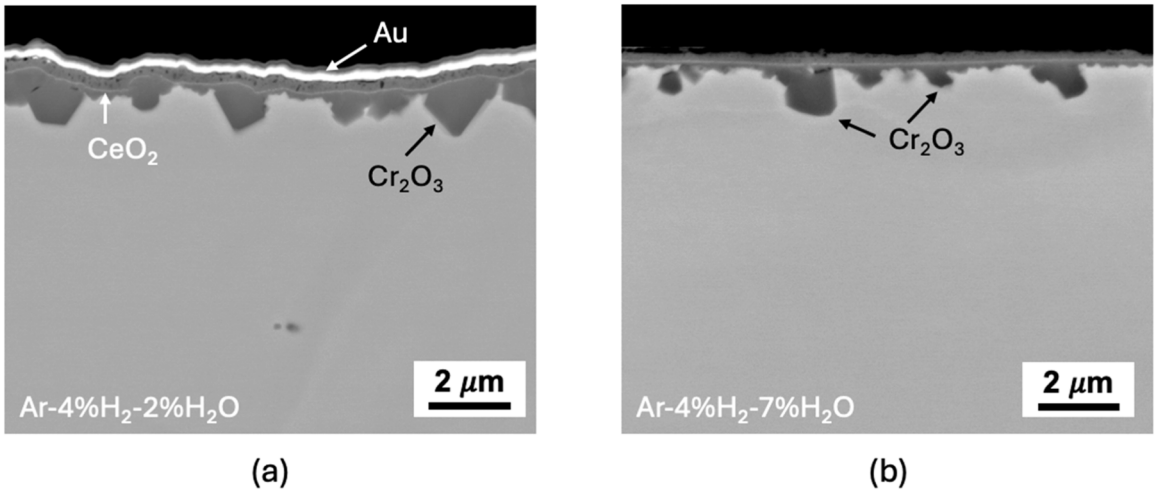

Fig. 4. BSE images of cross-sectioned Ce-coated Fe-18Cr specimens exposed for 72 h at 900 °C in (a) Ar-4 %H_2-2 %H_2O and (b) Ar-4 %H_2-7 %H_2O.

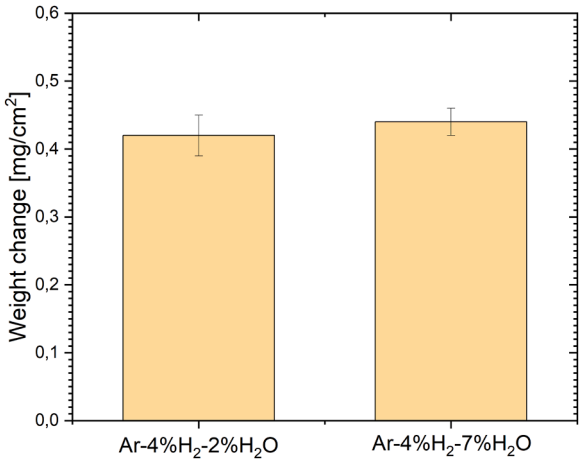

Fig. 5. Weight change of Fe-18Cr exposed for 72 h in Ar-4 %H_2-2 %H_2O and Ar-4 %H_2-7 %H_2O at 800 °C in a horizontal tube furnace.

3. Results

3.1. Breakaway oxidation of Fe-18Cr

3.1.1. Effect of pO_2

Fig. 1 shows *in-situ* recorded oxygen uptakes by Fe-18Cr exposed to Ar-4 %H_2-2 %H_2O and Ar-4 %H_2-7 %H_2O at 900 °C for 72 h. In Ar-4 %H_2-2 %H_2O in which FeO is thermodynamically unstable and cannot form (see Table 2), the weight gain by Fe-18Cr amounted to 1.3 mg/cm^2 in good agreement with available literature values for Fe-20Cr [12,25]. Exposure in Ar-4 %H_2-7 %H_2O resulted in a massive oxygen uptake of 26 mg/cm^2 indicating breakaway oxidation. BSE images in Fig. 2 demonstrate oxidation morphologies for Fe-18Cr exposed to Ar-4 %H_2-2 %H_2O (external Cr_2O_3 scale in Figs. 2**a**) and Ar-4 %H_2-7 %H_2O (breakaway oxidation Fig. 2**b**).

3.1.2. Effect of Ce-coating

The weight changes measured in furnace exposures at 900 °C for bare and Ce-coated Fe-18Cr are shown in Fig. 3. Oxygen uptakes for bare Fe-18Cr in the furnace exposures fully reproduced the values obtained in thermobalance. The oxygen uptakes for Ce-coated specimens were very low: 0.17 mg/cm^2 in Ar-4 %H_2-2 %H_2O and 0.29 mg/cm^2 in Ar-4 %H_2-7 %H_2O, respectively. A higher oxygen uptake in Ar-4 %H_2-7 %H_2O was due to a small nodule formed at the spot which was poorly coated with Ce in the PVD process, i.e., where the coupon was connected to the precut frame. Despite the nodule, the overall oxygen uptake by the Ce-coated specimen is two orders of magnitude lower than that of bare Fe-18Cr.

Fig. 4 demonstrates BSE images of oxide scales formed on the Ce-coated Fe-18Cr specimens exposed to Ar-4 %H_2-2 %H_2O (Figs. 4**a**) and Ar-4 %H_2-7 %H_2O (Fig. 4**b**) at 900 °C for 72 h. A thin string of bright CeO_2 precipitates marks the initial alloy surfaces. The oxide scale morphology is very similar for both atmospheres, i.e., a 300 nm thick outer scale is accompanied by 1–2 μm thick inwardly grown grains of Cr_2O_3. The Ce-doped oxide scale can be considered protective in both gases at 900 °C.

3.1.3. Effect of temperature

Fig. 5 shows oxygen uptakes by Fe-18Cr exposed to Ar-4 %H_2-2 %H_2O and Ar-4 %H_2-7 %H_2O at 800 °C in a horizontal tube furnace. The measured weight changes varied between 0.42 and 0.45 mg/cm^2 for both atmospheres. No indication of breakaway oxidation has been detected on all 8 specimens exposed at 800 °C.

Fig. 6 presents a collage of a panoramic BSE image of the Fe-18Cr specimen edge after 72 h exposure in Ar-4 %H_2-2 %H_2O and Ar-4 %H_2-7 %H_2O at 800 °C along with the high-magnification insets in the panoramic images highlighting the main oxidation morphology features: (i) the Cr_2O_3 scale on the specimen surface and (ii) the specimen edge. The specimen surfaces are uniformly covered by a 2.5 μm thick chromia layer in both atmospheres while the edges reveal different oxidation morphologies. In Ar-4 %H_2-2 %H_2O, the edges are covered with external Cr_2O_3. The oxygen potential in this gas is close to that of the Fe/FeO equilibrium at 800 °C (**see** Table 2). In Ar-4 %H_2-7 %H_2O, a continuous layer of Cr_2O_3 over the specimen edge is overlaid by a small nodule of Fe-rich oxide (FeO is stable in Ar-4 %H_2-7 %H_2O at 800 °C, see Table 2). Apparently, the FeO nodule had not grown further over the Cr_2O_3 subscale established underneath.

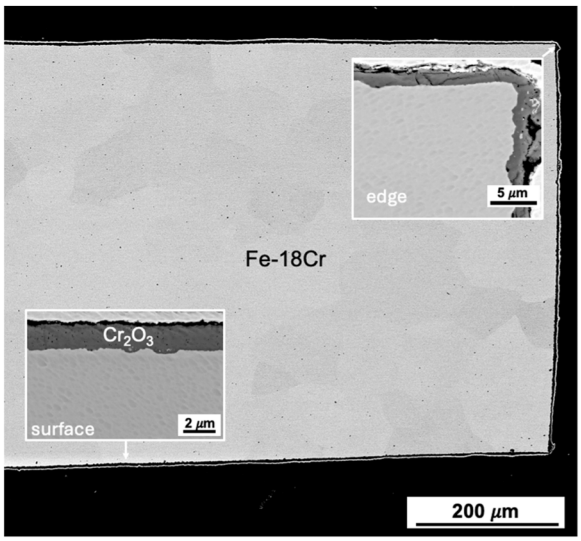

(a)

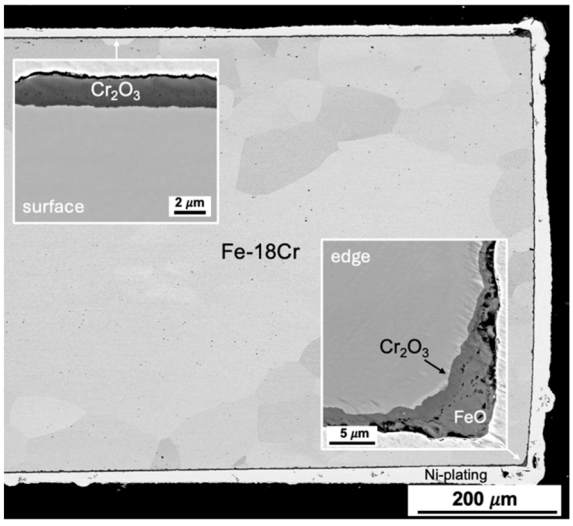

(b)

Fig. 6. BSE images of cross-sectioned Fe-18Cr specimen exposed for 72 h at 800 °C in (a) Ar-4 %H_2-2 %H_2O and (b) Ar-4 %H_2-7 %H_2O. The high magnification insets demonstrate different types of oxide scale morphologies in the same specimen.

3.1.4. Alloying effects

Fig. 7**a** summarizes the measured weight changes after furnace exposures at 900 °C in Ar-4 %H_2-2 %H_2O and Ar-4 %H_2-7 %H_2O for Fe-18Cr, Fe-30Cr, Fe-18Cr-2Mo and Fe-18Cr-0.5Si. A detailed view of the

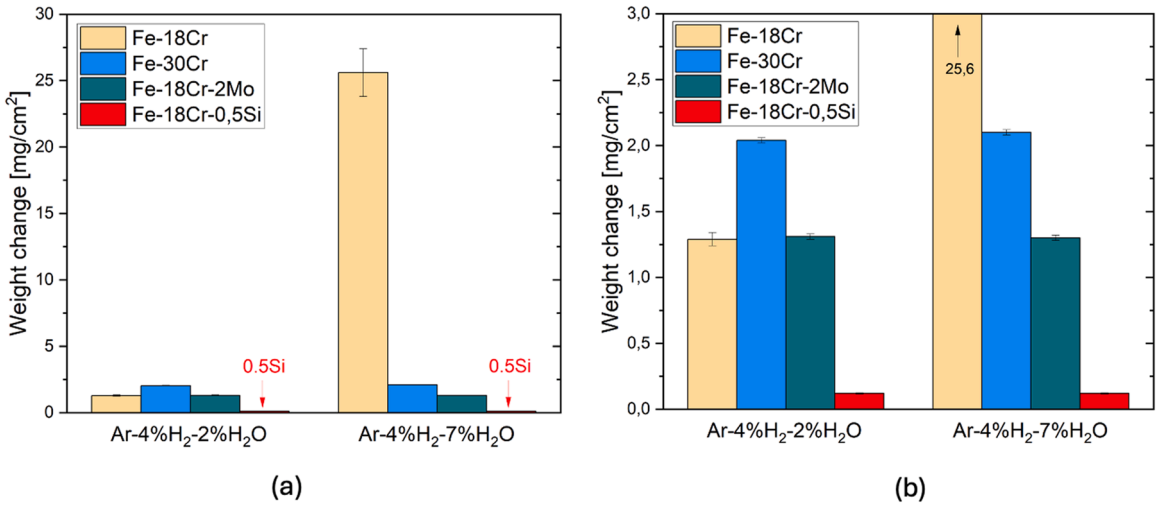

Fig. 7. Weight change of Fe-18Cr, Fe-30Cr, Fe-18Cr-2Mo and Fe-18Cr-0.5Si exposed for 72 h in Ar-4 %H_2-2 %H_2O and Ar-4 %H_2-7 %H_2O at 900 °C in a horizontal tube furnace.

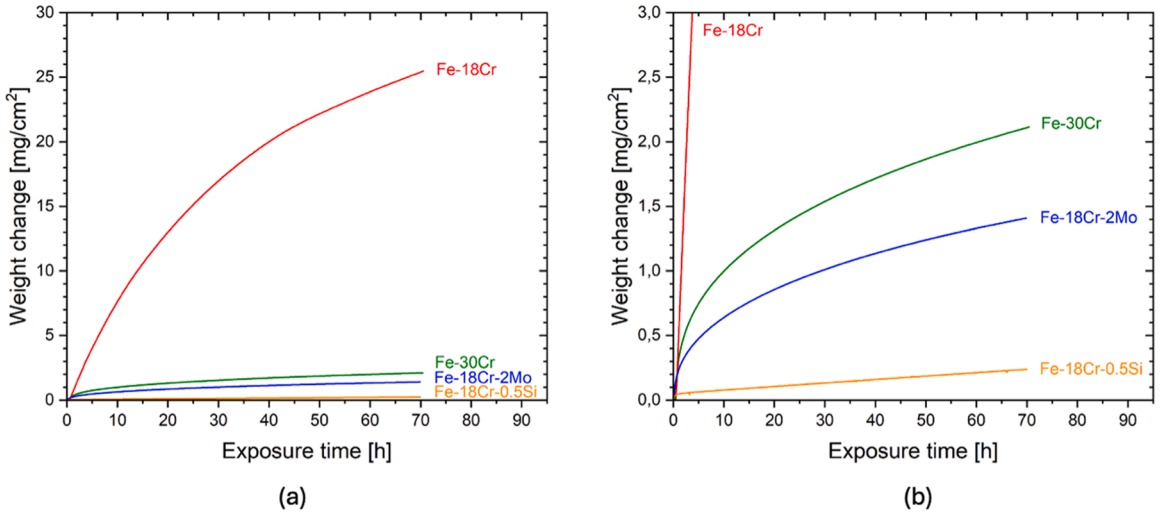

Fig. 8. In-situ weight change of Fe-18Cr, Fe-30Cr, Fe-18Cr-2Mo and Fe-18Cr-0.5Si exposed for 72 h to Ar-4 %H_2-7 %H_2O at 900 °C in thermobalance.

alloying effect on oxidation rates in Fig. 7**b** shows that

- Except for the Fe-18Cr reference alloy there was no substantial difference observed between Ar-4 %H_2-2 %H_2O (FeO is thermodynamically unstable) and Ar-4 %H_2-7 %H_2O (FeO is stable).
- alloying up to 30 %Cr resulted in a protective Cr_2O_3 scale and slightly higher mass gains in both atmospheres. This expected oxidation rate increase has been previously reported for binary FeCr-base alloys e.g. in [26].
- alloying with 2 %Mo did not affect the oxygen uptake in Ar-4 %H_2-2 %H_2O compared to unalloyed Fe-18Cr. In Ar-4 %H_2-7 %H_2O, the Mo addition drastically reduced the mass gain.
- Alloying with 0.5 %Si resulted in extremely low (0.13 mg/cm^2) mass gains in both atmospheres

The in-situ TG-curves in Fig. 8 demonstrate parabolic, diffusion-controlled oxidation kinetics for Fe-30Cr, Fe-18Cr-2Mo and Fe-18Cr-0.5Si and accurately reproduced the cumulative oxygen uptakes measured in the furnace exposures.

BSE images in Fig. 9 demonstrate oxides scales grown on Fe-18Cr (a), Fe-30Cr (b), Fe-18Cr-2Mo (c) and Fe-18Cr-0.5Si (d) after the exposure to Ar-4 %H_2-7 %H_2O (above FeO formation) for 72 h at 900 °C. Fe-18Cr grew a thick duplex oxide scale (see also Fig. 2**b**) while Fe-30Cr formed an external chromia scale (12 μm thick). A slightly thinner (8 μm thick) Cr_2O_3 scale was formed on Fe-18Cr-2Mo. The oxide scale on Fe-18Cr-0.5Si was duplex: a thin (0.5–1 μm thick) outer Cr_2O_3 scale is followed by an inner sublayer of SiO_2.

Low-magnification BSE images in Fig. 10 demonstrate the edges of the Fe-18Cr, Fe-30Cr, Fe-18Cr-2Mo, and Fe-18Cr-0.5Si specimens exposed for 72 h in Ar-4 %H_2-2 %H_2O and Ar-4 %H_2-7 %H_2O at 900 °C. Unalloyed Fe-18Cr suffered from internal oxidation in Ar-4 %H_2-2 %H_2O and breakaway oxidation in Ar-4 %H_2-7 %H_2O. Increasing Cr content to 30 wt% as well as alloying with Mo and Si resulted in a protective oxidation behavior in both gases.

Fig. 11 shows Cr depletion profiles measured by EDS in Fe-18Cr, Fe-18Cr-2Mo and Fe-18Cr-0.5Si after 72 h exposure at 900 °C in Ar-4 %H_2-2 %H_2O (empty symbols) and Ar-4 %H_2-7 %H_2O (full symbols). The effect of alloying Fe-18Cr with Mo and Si is demonstrated Fig. 11**a**. The interface Cr concentrations in the exposed specimens were extrapolated from the experimental depletion profiles: 13.1 wt% for uncoated Fe-18Cr (5.3 wt% Cr depletion), 12.5 wt% for Fe-18Cr-2Mo (5.9 wt% Cr depletion), 17.5 wt% for Fe-18Cr-0.5Si (0.9 wt% Cr depletion), and 17.6 wt% for Ce-coated Fe-18Cr (0.8 wt% Cr depletion, see Fig. 11**b**). The depletion depth is for both Fe-18Cr and Fe-18Cr-2Mo is

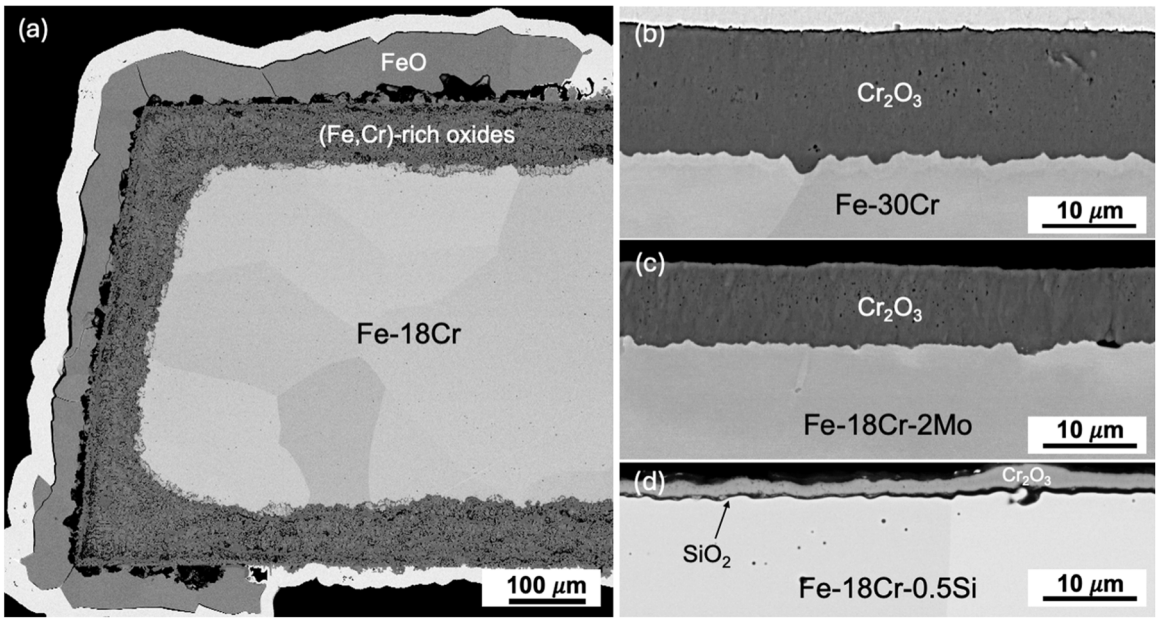

Fig. 9. BSE images of cross-sectioned Fe-18Cr (a), Fe-30Cr (b), Fe-18Cr-2Mo (c) and Fe-18Cr-0.5Si (d) specimens exposed for 72 h at 900 °C in Ar-4 %H_2-7 %H_2O.

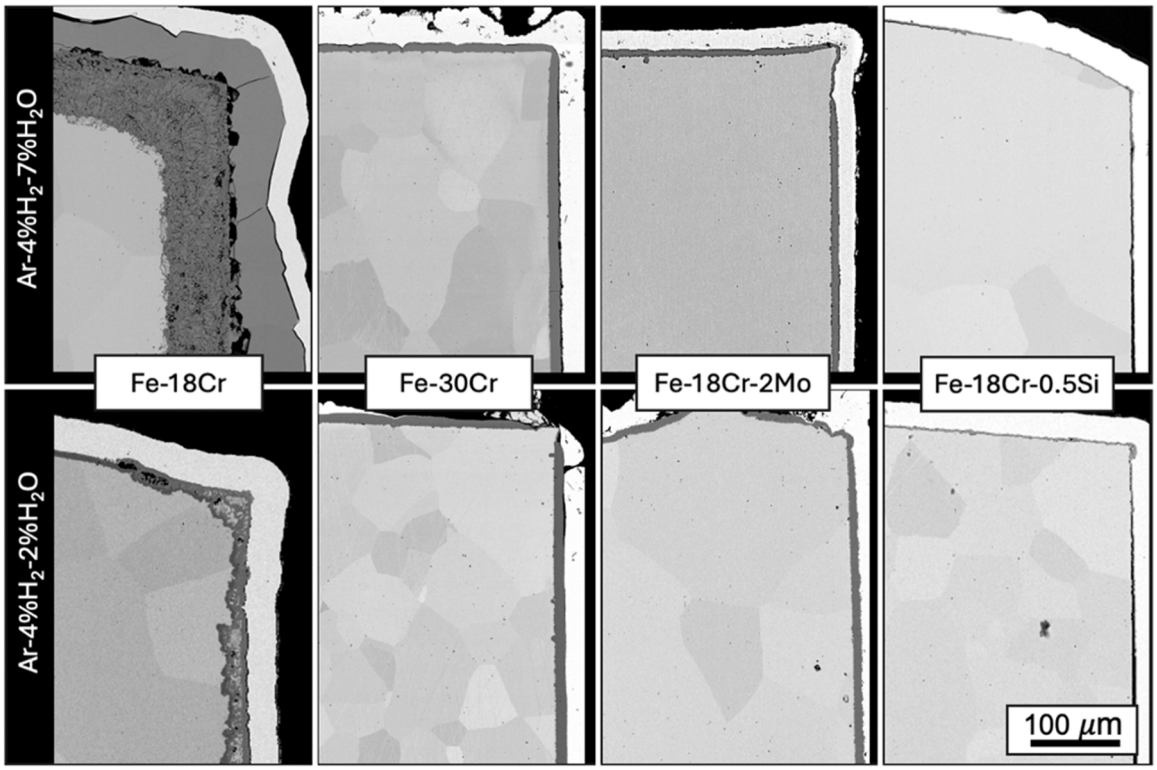

Fig. 10. BSE images showings edges of Fe-18Cr, Fe-30Cr, Fe-18Cr-2Mo and Fe-18Cr-0.5Si specimens exposed for 72 h at 900 °C in Ar-4 %H_2-2 %H_2O and Ar-4 %H_2-7 %H_2O.

approximately 90 μm. Alloying with 2 wt% Mo has thus no significant effect on Cr diffusion in Fe-18Cr at 900 °C.

The Cr depletion profile in Fe-18Cr-0.5Si is much flatter compared to those in Fe-18Cr and Fe-18Cr-2Mo due to a substantially lower oxide growth rate (see e.g. Fig. 7**b**). Ce-coating on Fe-18Cr has a very similar effect on Cr-depletion in Fe-18Cr as alloying with Si as suggested by oxygen uptakes (Fig. 3 and Fig. 7) and thicknesses of the Cr_2O_3 scale (Fig. 4 and Fig. 9). The Cr-depletion profiles are flat and uniform in the Ce-coated specimens compared to 5.3 wt% Cr depletion in bare Fe-18Cr irrespective of the exposure gas.

Fig. 12 demonstrates Cr depletion profiles in the exposed specimens of (a) Fe-30Cr, (b) Fe-18Cr-2Mo and (c) Fe-18Cr-0.5Si measured by EDS from surface as in Fig. 11 (blue symbols) and from the specimen edges (black symbols) after 72 h exposure at 900 °C in Ar-4 %H_2-2 %H_2O (empty symbols) and Ar-4 %H_2-7 %H_2O (full symbols). The Cr depletion profiles reveal a higher depletion of Cr at the edges of Fe-30Cr and Fe-18Cr-2Mo while the edges of Fe-18Cr-0.5Si were depleted of Cr as much as the surfaces. Clearly, this edge effect is augmenting with the

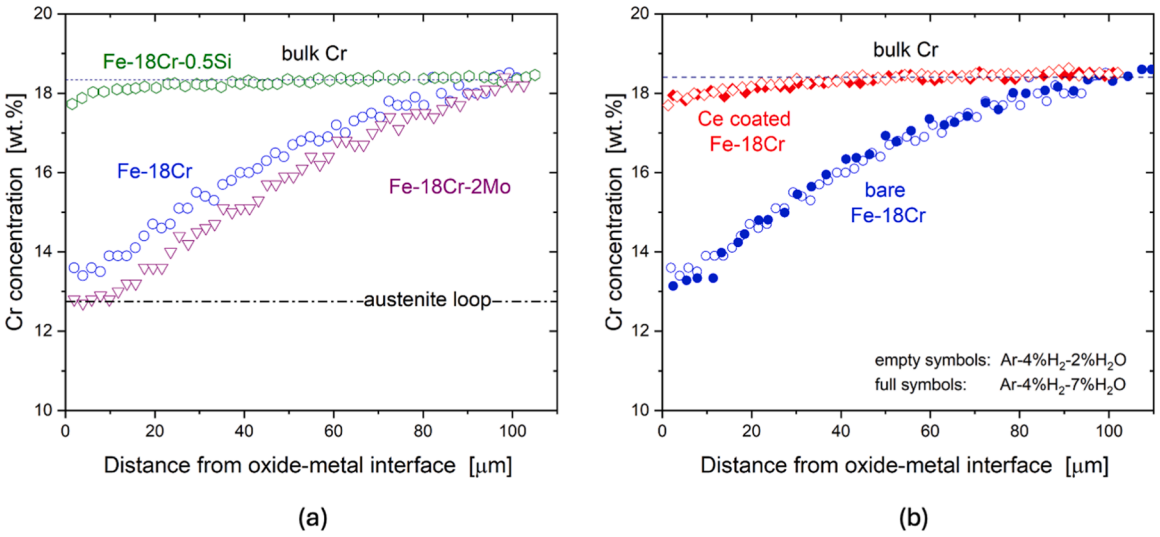

Fig. 11. Cr depletion profiles measured with EDS after 72 h exposure at 900 °C: (a) effect of alloying with Si and Mo; (b) effect of coating with Ce. Empty symbols denote exposures in Ar-4 %H_2-2 %H_2O, full symbols denote exposures in Ar-4 %H_2-7 %H_2O.

increasing oxidation rate, i.e., increasing Cr-consumption.

Fig. 13 compares Cr_2O_3 scales grown on Fe-18Cr (a) and Fe-18Cr-2Mo (b) at 900 °C in Ar-4 %H_2-2 %H_2O in the middle of the specimen. In agreement with the weight change measurements Fig. 7**b**, the Cr_2O_3 scales are morphologically similar and equally thick indicating thus a negligible effect of Mo addition on the oxide growth mechanism and oxidation rate.

Fig. 14 compares oxidation morphologies at the specimen edges of Fe-18Cr (a) and Fe-18Cr-2Mo (b) in Ar-4 %H_2-2 %H_2O at 900 °C. The Fe-18Cr specimen suffered from internal oxidation at the edges while the Mo-alloyed variant remained protective. As iron cannot oxidize externally in Ar-4 %H_2-2 %H_2O, internal oxidation is the only manifestation of the Cr_2O_3 scale failure.

Fig. 15 compares specimen edges of Fe-18Cr (a) and Fe-18Cr-2Mo (b) in Ar-4 %H_2-7 %H_2O at 900 °C. Above FeO formation, Fe-18Cr ran into breakaway forming a thick, duplex oxide scale at the edge while Fe-18Cr-2Mo retained a fully protective Cr_2O_3 scale all over the specimen.

4. Discussion

4.1. Austenitization hypothesis

What can be simpler than a binary alloy? This seeming simplicity of the Fe-Cr system is, however, highly misleading. In contrast e.g., to NiCr-base alloys [27], oxidation of FeCr-base alloys is affected by the following factors:

- Three different stable iron oxides FeO, Fe_3O_4, Fe_2O_3 along with Cr_2O_3 and $(Fe,Cr)_3O_4$ can form during oxidation
- Highly deficient, fast growing iron oxides (compared to NiO), whose growth rate is strongly affected by the atmosphere composition (pO_2).
- Various allotropic states of iron (α, γ and δ) with different diffusion transport properties.

The latter α-to-γ phase transformation has been rarely addressed in the literature on oxidation of FeCr-base alloys. In the available studies [10,22,28], it is mainly speculated that austenitization might be one fathomable explanation of breakaway oxidation at 900 °C and above. Up to date, there is no unanimous agreement on the role of oxidation-induced austenitization in oxidation of ferritic steels.

The proposed "high-temperature" breakaway mechanism is schematically presented in Fig. 16. Initially, the alloy surface is uniformly covered with the Cr_2O_3 scale (Fig. 16**a**). Due to a continuous Cr depletion from the alloy, the interface Cr-concentration drops from 18 to 13 wt% (Fig. 11), i.e., the concentration very close to the α/γ phase boundary (see the fragment of Fe-Cr phase diagram in Fig. 17).

The specimen edge is an area of a high surface-to-volume ratio [29,30], i.e., the alloy at the tip of the edge is being simultaneously depleted from two sides leading to a more substantial Cr-loss compared to the specimen center (Fig. 16**b**). In other words, the interface Cr concentration at the edge tip may fall below the stability limit of BCC leading to a nucleation of an austenitic grain (Fig. 16**c**, see also phase diagram in Fig. 17). Assuming that the Cr_2O_3 scaling process is unaffected by the phase transformation, i.e., the growth rates of Cr_2O_3 over the BCC and FCC alloy are identical, the slower diffusion of Cr in FCC would immediately deplete Cr at the edge tip to the level at which further Cr_2O_3 scaling cannot be maintained. A critical Cr depletion would then entail internal oxidation of Cr and (in atmospheres with sufficiently high oxygen activities) external oxidation of iron (Fig. 16**d**). This failure mechanism can be applied not only to the edges but to all surface defects such as particles of oxides, carbides, nitrides, etc. leading to sharp edges on the surfaces. In the following section, the proposed mechanism will be subjected to a classical diffusion analysis to quantitatively evaluate the feasibility of this scenario.

4.2. Diffusion analysis

The classical models of internal [31] and selective [32,33] oxidation proposed by Carl Wagner are often used to predict a transition from protective behavior to breakaway oxidation of FeCr- and NiCr-base alloys [12,34,35].

Wagner formulated two criteria to predict the (i) formation and (ii) maintenance of an external oxide scale growing on a binary alloy A-B, in which B reacts with oxygen to form oxide BO_μ while A is inert.

The first criterion, i.e., the scale formation criterion, given by Eq. (1), predicts the minimum concentration of B in the alloy necessary to suppress the inward ingress of oxygen dissolved in metal by counter-diffusion of B (Cr in the present study), thereby preventing internal oxidation.

$$N_B^{crit,1} > \left[\frac{\pi g^*}{3}\frac{\overline{V}_m}{\overline{V}_{ox}}\frac{N_O^{(s)}D_O}{\widetilde{D}_B}\right]^{\frac{1}{2}} \quad (1)$$

here $N_O^{(s)}$ is the oxygen solubility in the alloy in terms of mole-fraction,

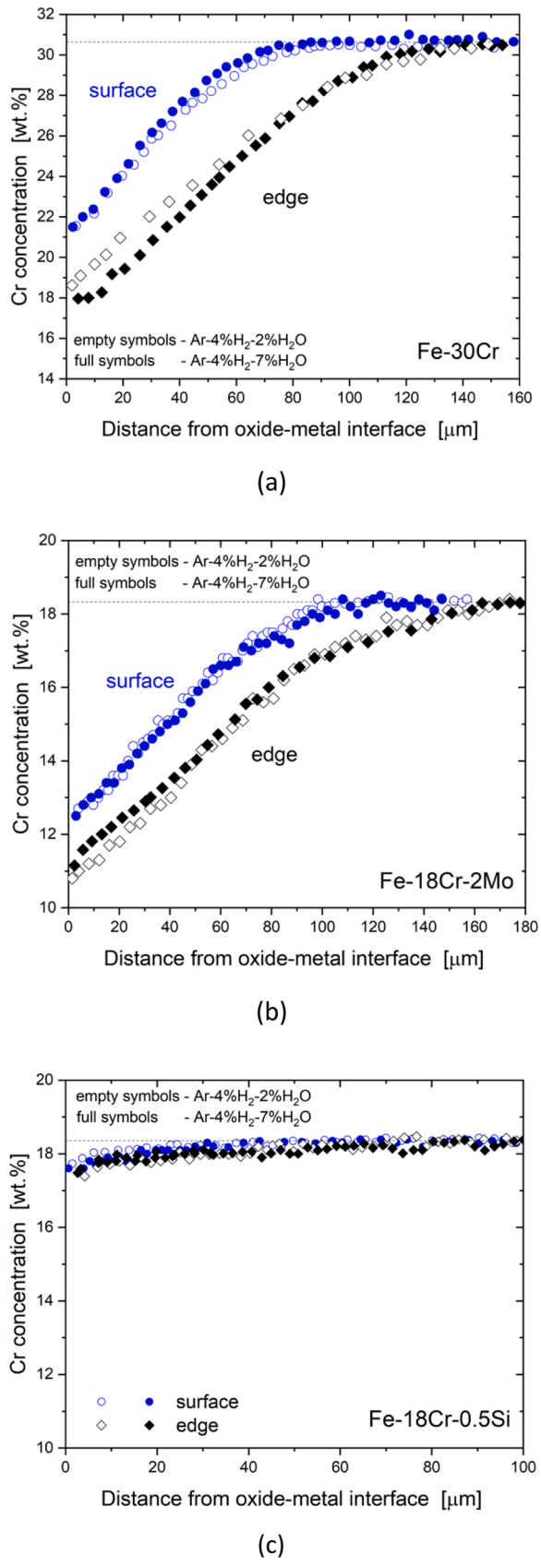

Fig. 12. Cr depletion profiles measured with EDS from specimen surface and specimen edges in (a) Fe-30Cr, (b) Fe-18Cr-2Mo and (c) Fe-18Cr-0.5Si after 72 h exposure in Ar-4 %H_2-2 %H_2O (empty symbols) and Ar-4 %H_2-7 %H_2O (full symbols) at 900 °C.

D_O is the diffusivity of oxygen in $m^2\ s^{-1}$, $\widetilde{D}_B$ is the interdiffusion coefficient of B in alloy A-B in $m^2\ s^{-1}$, $\overline{V}_m$ and $\overline{V}ox$ are the molar volumes of the alloy and oxide in $m^3\ mol^{-1}$, respectively. The internal oxide in the Fe-Cr system is generally assumed to be chromia, thus, the $\overline{V}_m$ and $\overline{V}_{ox}$ are 7 and 15 $cm^3\ mol^{-1}$, respectively. The factor g^* is the minimum volume-fraction of internal oxide required to start the transition from internal external to oxidation and has been approximated by Rapp [36] as 0.3.

The second Wagnerian criterion, i.e., the scale maintenance criterion, was derived from the depletion model and predicts the minimum Cr concentration, $N_B^{crit,2}$, in the alloy to sustain the flux of B towards the surface and thus maintain the protective oxide scale growth once it has been established. The second criterion is given as

$$N_B^{crit,2} > \left(\frac{\pi k_c}{2\widetilde{D}_B}\right)^{\frac{1}{2}} \tag{2}$$

where k_c is the parabolic rate constant in terms of metal recession in $m^2\ s^{-1}$.

In the present study, the k_c values are directly measured in our own experiments. The $\widetilde{D}_{Cr}$ values for BCC were taken from [22], and for FCC from [37]. The oxygen permeability, $N_O^{(s)}D_O$, data for both ferritic and austenitic iron were taken from the classical dataset by Swisher and Turkdogan [38].

The $N_{Cr}^{crit,1}$ and $N_{Cr}^{crit,2}$ values calculated for both BCC and FCC lattices at 900 °C are presented in Table 3 together with the input parameters and the experimental value of Cr depletion in the ferritic alloy (Fig. 11). The latter can be considered as experimental validation of $N_{Cr}^{crit,2}$ for BCC.

The $N_{Cr}^{crit,1}$ value for ferrite at 900 °C is predicted 0.093 or 8.7 wt% and thus the formation criterion is fulfilled for ferritic Fe-18Cr. The predicted $N_{Cr}^{crit,2}$ value (5.9 wt%) for BCC agrees very well with the experimentally measured Cr depletion (5.6 wt%). It is worth mentioning that the calculated and measured Cr interface concentration is extremely close to the α/γ phase boundary at 900 °C, i.e., 12.7 wt% (Fig. 17). It is evident that Cr depletion will be more intense at the edges of the specimens [29,39] where austenite formation is expected to start.

For the austenitic lattice, the predicted $N_{Cr}^{crit,1}$ and $N_{Cr}^{crit,2}$ values are much higher than the Cr content in the Fe-18Cr alloy, 22.8 and 31.8 wt %, respectively. The obvious reason for this is much slower Cr diffusion in the FCC lattice [37,40].

The Wagnerian criteria calculated for FCC clearly show that a hypothetical, FCC-base binary Fe-18Cr alloy can neither form nor sustain an external Cr_2O_3 scale. On the other hand, both criteria are fulfilled for ferritic Fe-18Cr. However, if an austenite grain/layer forms underneath the Cr_2O_3 scale, most likely at the edges of the specimen, the maintenance of the Cr_2O_3 scale will be disrupted leading to either internal oxidation (Fig. 14) or breakaway (Fig. 15) depending on the pO_2 of the atmosphere. Further theoretical analyses, especially 2D diffusion modeling of Cr depletion in the edges such as in [29,39], are needed to numerically validate this mechanism.

4.3. Experimental evidence supporting austenitization mechanism

(1) At 800 °C (Fig. 5), no substantial difference in oxidation rate is observed for Fe-18Cr between Ar-4 %H_2-2 %H_2O and Ar-4 %H_2-7 %H_2O because in both atmospheres a protective oxide scale is maintained. Irrespective of any local depletion effects, the material will never enter the γ-loop (Fig. 17). Just 100 °C higher at 900 °C, the situation is fundamentally different. Breakaway is observed in Ar-4 %H_2-7 %H_2O because now the Cr-depletion causes the α-to-γ transition.

(2) The Fe-30Cr alloys behave highly similar in both atmospheres because the depletion is not sufficient to approach the γ-loop

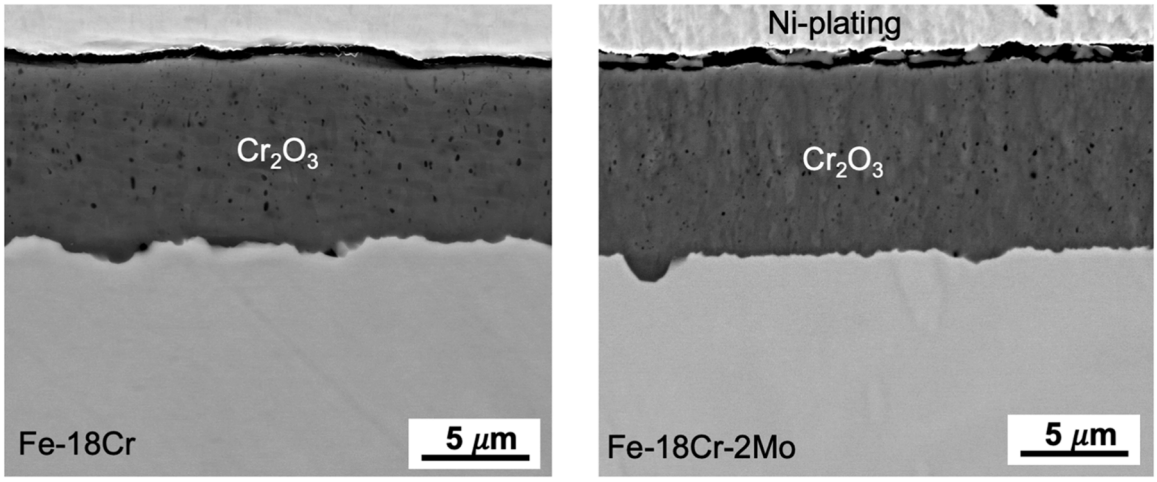

Fig. 13. BSE images of cross-sectioned Fe-18Cr (a) and Fe-18Cr-2Mo (b) after 72 h exposure at 900 °C in Ar-4 %H_2-2 %H_2O. The images were taken in the middle of the specimen.

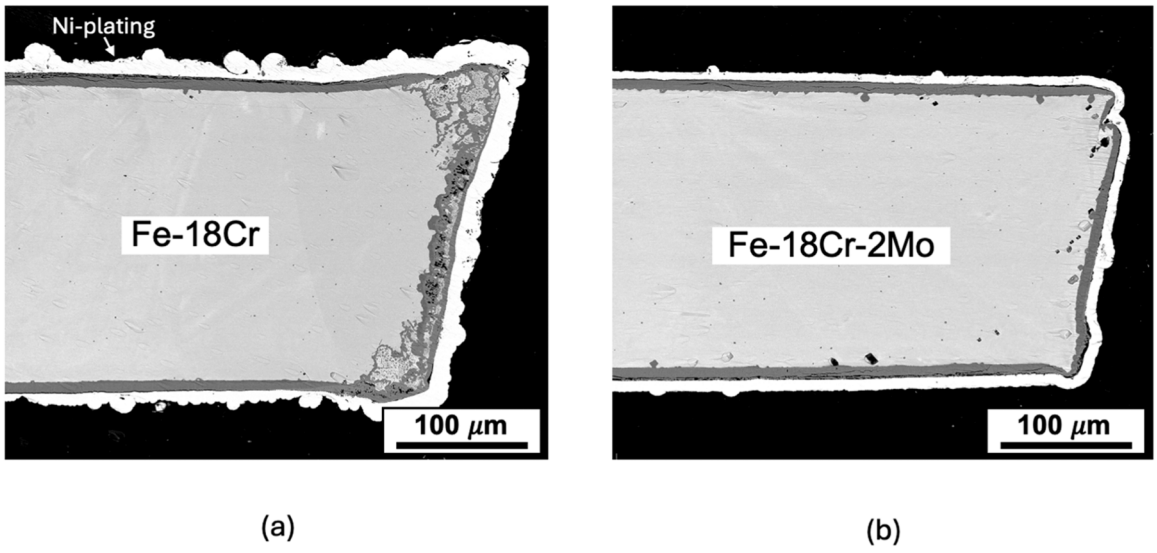

Fig. 14. BSE images of cross-sectioned Fe-18Cr (a) and Fe-18Cr-2Mo (b) after 72 h exposure at 900 °C in Ar-4 %H_2-2 %H_2O (below FeO formation). The images were taken at the edge of the specimen.

(Fig. 17) and start the α-to-γ transition even at the edges (Fig. 12a).

(3) The addition of Mo has no direct effect on oxidation rate (compare Fig. 13). Nevertheless, Mo has a profound impact on the oxidation rate in Ar-4 %H_2-7 %H_2O. This is caused by the ferrite stabilizing effect of Mo.

(4) The addition of Si has a twofold effect. It reduces the oxidation rate so that the Cr depletion is not sufficient to cause the α-to-γ transition, furthermore the α phase is stabilized. It should be noted that the γ-loop shrinkage by alloying Fe-Cr with 0.5 wt% Si is much weaker compared to alloying with Mo (Fig. 17). Therefore, the primary beneficial effect of Si is based on lowering the oxidation rate.

(5) The Ce coating completely differentiates these two effects as it does not affect phase stabilities in the alloy but has a direct impact on the oxidation rate, lowering it to an extent that depletion becomes minimal (Fig. 11).

4.4. *Factors facilitating breakaway oxidation*

Breakaway oxidation of ferritic Fe-Cr based alloys at 900 °C is triggered by austenitization which, in turn, is the result of Cr-depletion. In this regard, the exposure atmosphere is not the main factor as Cr-depletion occurs irrespective of the oxidant. Another important trigger of an early onset of breakaway oxidation in ferritic steels is a lower Cr content, i.e., the closer to the austenite loop (Fig. 17) the higher is the risk of failure providing that the alloy does not contain ferrite stabilizers such as W, Nb, Mo, Si [10].

Cr-depletion can be further intensified by i) reactive Cr-evaporation in wet gases [14,15], oxide spallation resulting from thermal cycling [41] and/or iii) a lower Cr-reservoir due to geometrical constraints (e.g., thin foils, wires, metal foams) [42,43]. At 900 °C and above, all these phenomena are likely to promote breakaway oxidation at sharp edges of an exposed part and its further lateral propagation over the surface (Fig. 13).

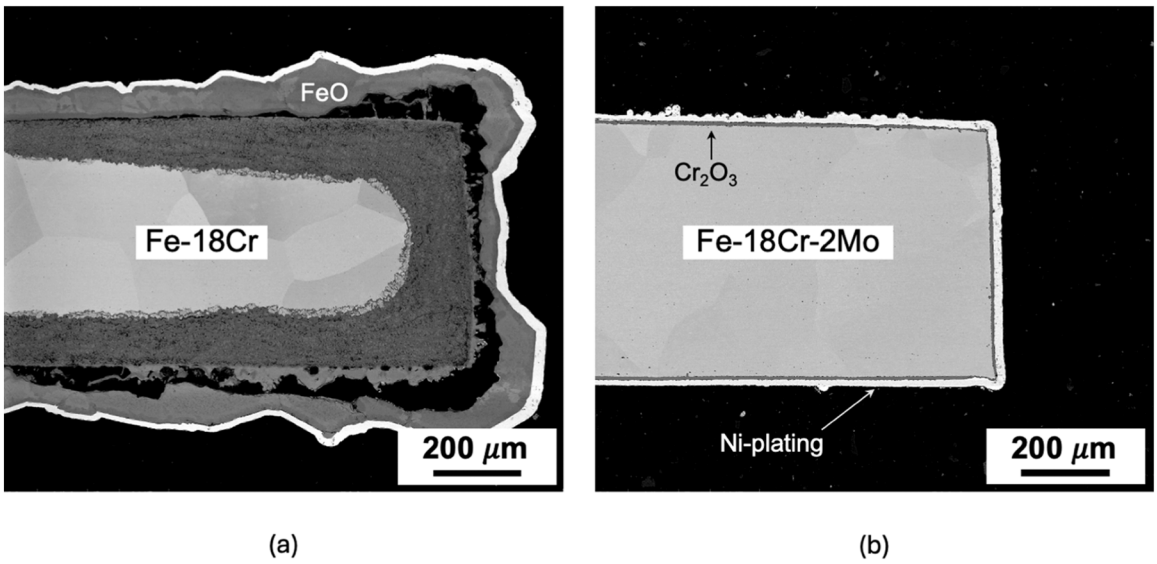

Fig. 15. BSE images of cross-sectioned Fe-18Cr (a) and Fe-18Cr-2Mo (b) after 72 h exposure at 900 °C in Ar-4 %H_2-7 %H_2O (above FeO formation). The images were taken at the edge of the specimen.

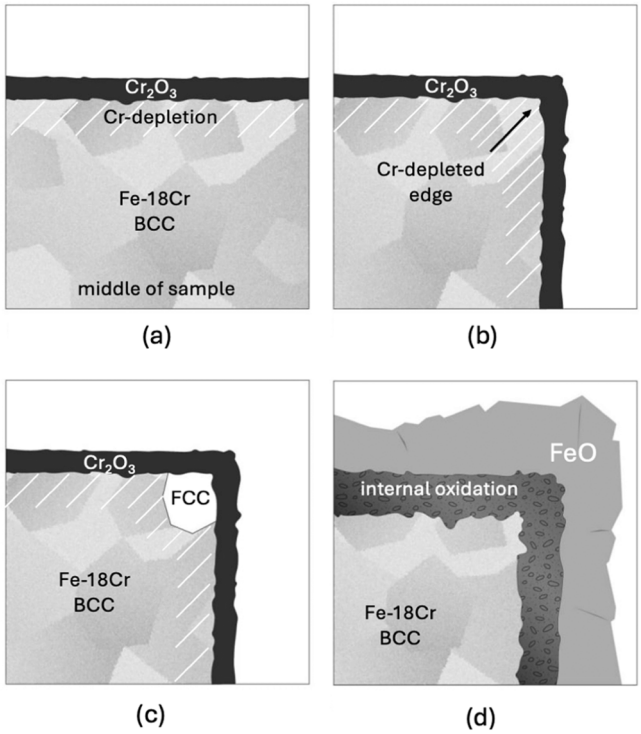

Fig. 16. Schematic of breakaway mechanism in Fe-Cr alloys at 900 °C: (a) protective scaling of Cr_2O_3 in the middle of sample, (b) Cr depletion at the specimen edge, (c) nucleation of FCC grain, d) breakaway oxidation.

4.5. Mitigation strategies

In the present study, experiments were undertaken to avoid the austenitization scenario in ferritic Fe-Cr based alloys:

- Lowering exposure temperature to 800 °C to stay beneath the austenite loop
- Increasing Cr content to 30 wt% to prevent critical Cr depletion at the edges
- Coating with Ce to lower the oxidation rate
- Alloying with Si to form a subscale of SiO_2 and thus lower Cr consumption/depletion
- Alloying with Mo to completely suppress austenitization at 900 °C

All these experiments resulted in a protective, non-breakaway behavior of the tested FeCr-base alloys and thus corroborate the proposed "high-temperature" breakaway mechanism based on austenitization. On the other hand, these experiments provide practical recommendations for alloy design and/or material selection.

Steels alloyed with ferrite stabilizers (W, Mo, Nb, Si) and/or coated/doped with reactive elements (RE) are generally less likely to suffer from breakaway oxidation at 900 °C than their unalloyed/uncoated counterparts.

When considering the role of ferrite stabilizers, care should be taken as some of them might, depending on their contents, affect the oxide scale growth. For instance, Ti and Nb, when present in sufficiently high concentrations in the steel might increase the chromia scale growth rate by p-type doping or formation of oxide grain-boundary structures allowing fast diffusion [44].

Alloying additions of elements acting as ferrite stabilizers that simultaneously reduce the scale growth rate, such as Si forming a silica sub-scale, are beneficial [45]. Unfortunately, high Si additions are not practical due to embrittlement of the steel. With additions below 1 % the positive effect of Si is mainly related to reduction of scaling rate (Fig. 9).

Minor reactive element (RE) additions such as Ce dramatically reducing the chromia scale growth rate are another approach. It was shown that RE-additions suppress cation diffusion in chromia (and alumina) scales [46]. Fig. 4 indicates that the chromia scale on the Ce-coated steel is very thin and its growth is accompanied by local formation of intrusions, which apparently grew by oxygen inward transport thereby supporting the earlier suggested mechanism. The exact reason for the formation of intrusions is not understood and requires further investigation beyond the scope of the present paper. It might be related for example to an effect of Ce-coating on nucleation of new chromia grains.

The RE-additions can be implemented as coatings (as shown in the present work with Ce-oxide) as well as alloying constituents. In the latter case, it is important to consider that the RE-effect depends on the free RE-reservoir rather than content. The free RE-reservoir can in turn be affected by the contents of alloy impurities, such as S, O or C as well by component (specimen) thickness as shown for alumina forming alloys and coatings [46]. It should be also kept in mind that too high

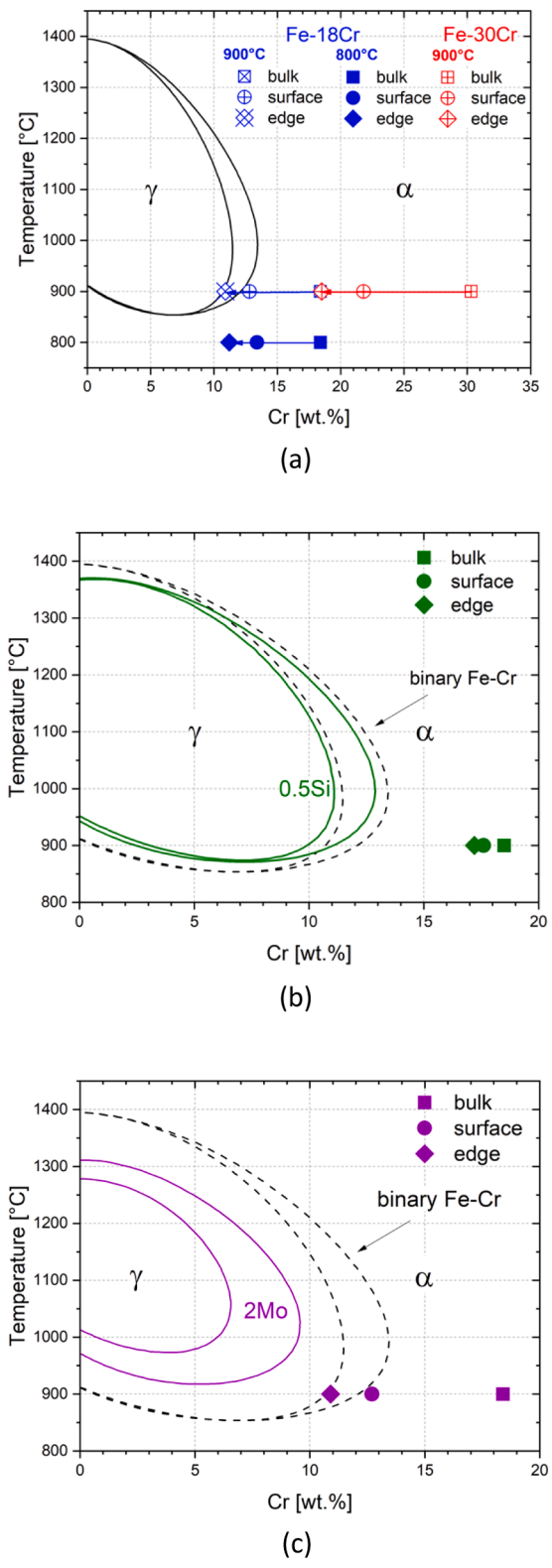

Fig. 17. Fragment of binary Fe-Cr phase diagram (a) demonstrating effects of alloying Fe-Cr with 0.5 wt% Si (b) and 2 wt% Mo (c) on the γ-loop (black dashed lines) calculated in Thermo-Calc using TCFE9 database. Symbols denote average Cr concentrations measured with EDS in specimen bulk (squares), at oxide-metal interface (circles) and at specimen edge (rhombs). Datapoint for specimen edge of Fe-18Cr at 900 °C in figure (a) is the measurement for Fe-18Cr-2Mo.

RE-contents (reservoirs) might lead to so-called overdoping [46] and the resulting oxidation rate might be higher than that of the steels with moderate RE-additions.

Another mitigation strategy is related to component geometry. Thereby sharp edges, corners and holes should be avoided in the ferritic steel components to prevent local austenitization if alloying with ferrite stabilizers and/or RE-coatings is not an option.

5. Conclusions

The present study proposed and experimentally validated the austenitization mechanism explaining breakaway oxidation of borderline ferritic stainless steels containing 16–18 wt% of Cr exposed to H_2/H_2O environments at 900 °C. The following conclusions need to be highlighted:

- Binary Fe-18Cr is sensitive to the oxygen potential of the H_2/H_2O mixture at 900 °C. In Ar-4 %H_2-2 %H_2O in which FeO is thermodynamically unstable, Fe-18Cr tends to form an external Cr_2O_3 scale. At the same time, the specimen edges are prone to internal oxidation attack. In Ar-4 %H_2-7 %H_2O in which Fe can oxidize externally, Fe-18Cr suffers from intense breakaway oxidation mainly at the specimen edges.
- The observed breakaway oxidation at 900 °C in Ar-4 %H_2-7 %H_2O is an evident edge effect although several FeO nodules were observed on the specimen faces. Oxidation-driven Cr depletion of the specimen edges induces the α-to-γ transformation and results in either internal attack or in catastrophic breakaway oxidation.
- Wagnerian diffusion analysis predicts a protective behavior for Fe-18Cr as long as the alloy remains ferritic. Formation of an austenite grain/layer is predicted to disrupt Cr supply to the alloy surface and thus undermine protectiveness of the Cr_2O_3 scale.
- Alloying with Si and/or coating Fe-18Cr with 10 nm Ce results in a dramatic decrease of the oxidation rate (k_p) suppressing the outward transport of Cr cations and thus breakaway oxidation.
- An alternative way to suppress austenitization and thus breakaway at 900 °C is alloying with ferrite stabilizers as shown in this work using Mo. Molybdenum does not affect the oxidation rate of FeCr but it completely prevents the alloy from running into breakaway oxidation even in Ar-4 %H_2-7 %H_2O.
- Commercially available ferritic steels containing ferrite stabilizers and/or Si are less likely to suffer from breakaway oxidation at 900 °C compared to the unalloyed grades. Smart alloying of the Fe-Cr system can fully prevent breakaway oxidation at 900 °C. A better oxidation resistance can be achieved through different alloying strategies and is subject to future design and development of ferritic stainless.

Author statement

All persons who meet authorship criteria are listed as authors, and all authors certify that they have participated sufficiently in the work to take public responsibility for the content, including participation in the concept, design, analysis, writing, or revision of the manuscript. Furthermore, each author certifies that this material or similar material has not been and will not be submitted to or published in any other publication before its appearance in *Corrosion Science*.

Declaration of Competing Interest

The authors declare that they have no known competing financial interests or personal relationships that could have appeared to influence the work reported in this paper.

Table 3
Literature data and calculated $N_{Cr}^{crit,1}$ and $N_{Cr}^{crit,2}$ for ferritic (BCC) austenitic (FCC) binary Fe-Cr system at 900 °C. The oxygen solubility and diffusivity data are taken from [38], Cr diffusion coefficients were taken from [22] for BCC and from [37] for FCC. Oxidation rates were determined from own experimental results.

lattice	$N_O^{(s)}$	D_O (m^2s^{-1})	$\widetilde{D}_{Cr}$	k_c (m^2s^{-1})	$N_{Cr}^{crit,1}$	$N_{Cr}^{crit,2}$	$N_{Cr}^{crit,2}$exp
BCC	3.0×10^{-6}	1.7×10^{-10}	9.0×10^{-15}	1.8×10^{-18}	0.093	0063	0.060
FCC	6.8×10^{-6}	1.8×10^{-11}	3.0×10^{-16}	1.8×10^{-18}	0.241	0333	-

Acknowledgments

All persons who have made substantial contributions to the work reported in the manuscript (e.g., technical help, writing and editing assistance, general support), but who do not meet the criteria for authorship, are named in the Acknowledgments and have given us their written permission to be named. If we have not included an Acknowledgments, then that indicates that we have not received substantial contributions from non-authors. This work was funded by the European Union, project MSCA4Ukraine, grant No. 1232975. The present publication reflects only the author's views, and the European Union is not liable for any use that may be made of the information contained therein. Mr. H. Cosler is acknowledged for performing the TG-experiments and Mr. E. Wessel for a part of the SEM analysis, respectively.

Data availability

Data will be made available on request.

References

[1] B. Pujilaksono, T. Jonsson, H. Heidari, M. Halvarsson, J.-E. Svensson, L.-G. Johansson, Oxidation of binary FeCr alloys (Fe–2.25Cr, Fe–10Cr, Fe–18Cr and Fe–25Cr) in O2 and in O2 + H2O environment at 600 °C, Oxid. Met. 75 (2011) 183–207.
[2] N.K. Othman, J. Zhang, D.J. Young, Water vapour effects on Fe-Cr alloy oxidation, Oxid. Met. 73 (2010) 337–352.
[3] N. Mu, K. Jung, N.M. Yanar, et al., The effects of water vapor and hydrogen on the high-temperature oxidation of alloys, Oxid. Met. 79 (2013) 461–472.
[4] M. Schütze, D. Renusch, M. Schorr, Parameters determining the breakaway oxidation behaviour of ferritic martensitic 9%Cr steels in environments containing H2O, Corros. Eng., Sci. Technol. 39 (2004) 157–166.
[5] H. Asteman, K. Segerdahl, J.E. Svensson, et al., Oxidation of stainless steel in H2O/O2 environments - role of chromium evaporation, in: P. Steinmetz, I.G. Wright, G. Meier, A. Galerie, B. Pieraggi, R. Podor (Eds.), High Temperature Corrosion and Protection of Materials 6, Prt 1 and 2, Proceedings, 461–464, 2004, pp. 775–782.
[6] R. Sachitanand, J.E. Svensson, J. Froitzheim, The influence of Cr evaporation on long term Cr depletion rates in ferritic stainless steels, Oxid. Met. 84 (2015) 241–257.
[7] R. Sachitanand, M. Sattari, J.-E. Svensson, J. Froitzheim, Evaluation of the oxidation and Cr evaporation properties of selected FeCr alloys used as SOFC interconnects, Int J. Hydrog. Energy 38 (2013) 15328–15334.
[8] J. Ehlers, D.J. Young, E.J. Smaardijk, et al., Enhanced oxidation of the 9%Cr steel P91 in water vapour containing environments, Corros. Sci. 48 (2006) 3428–3454.
[9] T.D. Nguyen, J. Zhang, D.J. Young, Effects of H2 on microstructures of Cr2O3 scales grown in water vapour and consequences for breakaway, Corros. Sci. 236 (2024) 112265.
[10] D.J. Young, J. Zurek, L. Singheiser, W.J. Quadakkers, Temperature dependence of oxide scale formation on high-Cr ferritic steels in Ar-H2-H2O, Corros. Sci. 53 (2011) 2131–2141.
[11] A. Chyrkin, K.O. Gunduz, V. Asokan, J.-E. Svensson, J. Froitzheim, High temperature oxidation of AISI 441 in simulated solid oxide fuel cell anode side conditions, Corros. Sci. 203 (2022) 110338.
[12] E. Essuman, G.H. Meier, J. Zurek, M. Hänsel, W.J. Quadakkers, The effect of water vapor on selective oxidation of Fe-Cr alloys, Oxid. Met. 69 (2008) 143–162.
[13] E. Essuman, G.H. Meier, J. Zurek, M. Hänsel, L. Singheiser, W.J. Quadakkers, Enhanced internal oxidation as trigger for breakaway oxidation of Fe-Cr alloys in gases containing water vapor, Scr. Mater. 57 (2007) 845–848.
[14] H. Asteman, J.E. Svensson, L.G. Johansson, Evidence for chromium evaporation influencing the oxidation of 304L: the effect of temperature and flow rate, Oxid. Met. 57 (2002) 193–216.
[15] G.R. Holcomb, Calculation of reactive-evaporation rates of chromia, Oxid. Met. 69 (2008) 163–180.
[16] D.J. Young, B.A. Pint, Chromium volatilization rates from Cr2O3 scales into flowing gases containing water vapor, Oxid. Met. 66 (2006) 137–153.
[17] M. Stanislowski, J. Froitzheim, L. Niewolak, et al., Reduction of chromium vaporization from SOFC interconnectors by highly effective coatings, J. Power Sources 164 (2007) 578–589.
[18] M.J. Reddy, B. Kamecki, B. Talic, et al., Experimental review of the performances of protective coatings for interconnects in solid oxide fuel cells, J. Power Sources 568 (2023) 232831.
[19] P. Alnegren, M. Sattari, J.E. Svensson, J. Froitzheim, Temperature dependence of corrosion of ferritic stainless steel in dual atmosphere at 600-800 °C, J. Power Sources 392 (2018) 129–138.
[20] P. Alnegren, M. Sattari, J.E. Svensson, J. Froitzheim, Severe dual atmosphere effect at 600 °c for stainless steel 441, J. Power Sources 301 (2016) 170–178.
[21] K.O. Gunduz, A. Chyrkin, C. Goebel, et al., The effect of hydrogen on the breakdown of the protective oxide scale in solid oxide fuel cell interconnects, Corros. Sci. 179 (2021) 109112.
[22] D.P. Whittle, G.C. Wood, D.J. Evans, D.B. Scully, Concentration profiles in the underlying alloy during the oxidation of iron-chromium alloys, Acta Metall. 15 (1967) 1747–1755.
[23] M.J. Reddy, J.-E. Svensson, J. Froitzheim, Reevaluating the Cr evaporation characteristics of Ce/Co coatings for interconnect applications, ECS Trans. 103 (2021) 1899–1905.
[24] I. Barin, Thermochemical Data of Pure Substances, Wiley, 1995, https://doi.org/10.1002/9783527619825.
[25] L. Mikkelsen, S. Linderoth, High temperature oxidation of Fe–Cr alloy in O2–H2–H2O atmospheres; microstructure and kinetics, Mater. Sci. Eng.: A 361 (2003) 198–212.
[26] G.R. Wallwork, The oxidation of alloys, Rep. Prog. Phys. 39 (1976) 401.
[27] J. Zurek, G.H. Meier, E. Essuman, M. Hänsel, L. Singheiser, W.J. Quadakkers, Effect of specimen thickness on the growth rate of chromia scales on Ni-base alloys in high- and low-pO2 gases, J. Alloy. Compd. 467 (2009) 450–458.
[28] J. Zurek, G.H. Meier, E. Wessel, L. Singheiser, W.J. Quadakkers, Temperature and gas composition dependence of internal oxidation kinetics of an Fe-10%Cr alloy in water vapour containing environments, Mater. Corros. 62 (2011) 504–513.
[29] W.M. Pragnell, H.E. Evans, Chromium depletion at 2-dimensional features during the selective oxidation of a 20Cr-25Ni austenitic steel, Oxid. Met. 66 (2006) 209–230.
[30] Quadakkers W.J., Naumenko D., Weinbruch S., Gurrappa I. Factors governing breakaway oxidation of FeCrAl-based alloys Bestimmende Einflußgro È ßen fu È r die katastrophale Oxidation von FeCrAl-Legierungen. doi:10.1002/(SICI)1521-4176(200004)51:4.
[31] C. Wagner, Reaktionstypen bei der Oxydation von Legierungen, Z. fur Elektrochem. 63 (1959) 772–790.
[32] C. Wagner, Theoretical analysis of the diffusion processes determining the oxidation rate of alloys, J. Electrochem Soc. 99 (1952) 369.
[33] C. Wagner, Oxidation of alloys involving noble metals, J. Electrochem Soc. 103 (1956) 571.
[34] E. Essuman, G.H. Meier, J. Zurek, et al., Protective and non-protective scale formation of NiCr alloys in water vapour containing high- and low-pO2 gases, Corros. Sci. 50 (2008) 1753–1760.
[35] G.H. Meier, K. Jung, N. Mu, et al., Effect of alloy composition and exposure conditions on the selective oxidation behavior of ferritic Fe-Cr and Fe-Cr-X alloys, Oxid. Met. 74 (2010) 319–340.
[36] R.A. Rapp, The transition from internal to external oxidation and the formation of interruption bands in silver-indium alloys, Acta Metall. 9 (1961) 730–741.
[37] P.I. Williams, R.G. Faulkner, Chemical volume diffusion coefficients for stainless steel corrosion studies, J. Mater. Sci. 22 (1987) 3537–3542.
[38] J.H. Swisher, E.T. Turkdogan, Solubility, permeability and diffusivity of oxygen in solid iron, Trans. Metall. Soc. 239 (1967) 426–431.
[39] W.M. Pragnell, H.E. Evans, A finite-difference model to predict 2D depletion profiles arising from high temperature oxidation of alloys, Model Simul. Mater. Sci. Eng. 14 (2006) 733–740.
[40] P.J. Alberry, C.W. Haworth, Interdiffusion of Cr, Mo, and W in Iron, Met. Sci. 8 (1974) 407–412.
[41] J.L. Smialek, A deterministic interfacial cyclic oxidation spalling model, Acta Mater. 51 (2003) 469–483.
[42] D. Koszelow, M. Makowska, F. Marone, J. Karczewski, P. Jasiński, S. Molin, High temperature corrosion evaluation and lifetime prediction of porous Fe22Cr stainless steel in air in temperature range 700–900 °C, Corros. Sci. 189 (2021) 109589.
[43] P. Huczkowski, N. Christiansen, V. Shemet, J. Piron-Abellan, L. Singheiser, W. J. Quadakkers, Oxidation limited life times of chromia forming ferritic steels, Mater. Corros. 55 (2004) 825–830.
[44] A. Vayyala, I. Povstugar, D. Naumenko, W.J. Quadakkers, H. Hattendorf, J. Mayer, Effect of gas composition on the oxide scale growth mechanisms in a ferritic steel for solid oxide cell interconnects, Corros. Sci. 221 (2023) 111317.
[45] F.H. Stott, G.J. Gabriel, G.C. Wood, The influence of silicon on the high-temperature oxidation of nickel, Oxid. Met. 28 (1987) 329–345.
[46] D. Naumenko, B.A. Pint, W.J. Quadakkers, Current thoughts on reactive element effects in alumina-forming systems: in memory of john stringer, Oxid. Met. 86 (2016) 1–43.